Electric Supplemental Information:

Large negative thermal expansion in non-perovskite lead-free ferroelectric $Sn_2P_2S_6$

Yangchun Rong,[1] Menglei Li,[2] Jun Chen,[1] Mei Zhou,[2] Kun Lin,[1] Lei Hu,[1] Wenxia Yuan,[3] Wenhui Duan,[2] Jinxia Deng,[3] Xianran Xing [1*]

[1] Department of Physical Chemistry, [3] Department of Chemistry and Chemical Engineering, University of Science and Technology Beijing, Beijing 100083, China

[2] Department of Physics and State Key Laboratory of Low-Dimensional Quantum Physics, Tsinghua University, Beijing 100084, China

1. Preparation of $Sn_2P_2S_6$ powders

The $Sn_2P_2S_6$ powders with high crystallization and purity were synthesized using SnS and "P_4S_8". The "P_4S_8" was obtained by a reaction of red phosphorus with sulfur at 620 K in evacuated quartz tube. Then 0.30 g SnS and 0.22 g "P_4S_8" (~ 20% excess) were grounded carefully and sealed in evacuated quartz tube (10 mm$\times\Phi$ 8 mm). The tube was then put into a hot furnace of 750-820 K to proceed rapid heating and keep for six hours. The obtained $Sn_2P_2S_6$ powders display yellowish brown color at room temperature.

2. DSC, SEM characterization and Raman spectrum of prepared powders

The Scanning Electron Microscope (SEM) was carried out with a Zeiss Supra55 to study the grain size of as-prepared powders. Figure S1 shows the typical grain size is above 2 μm, indicates a good crystallization.

The Differential Scanning Calorimetry (DSC) was carried out with a PerkinElmer DSC8500 calorimeter to investigate the phase transition temperature of the synthesized $Sn_2P_2S_6$ powders. The scanning rate was 5 K/min from 170 K to 420 K. Figure S2 clearly shows a peak of heat flow around 338 K, corresponding to the second-order phase transition and consistent well with the reported 339 K from single crystals.[1]

To further confirm the $Sn_2P_2S_6$ phase, Raman spectrum was also carried out at room temperature with a Jobin–Yvon LabRAM HR 800 UV micro-Raman system (632.8 nm, He–Ne laser) in back-scattering geometry from 50 cm^{-1} to 800 cm^{-1}. Figure S3 shows that the sharp Raman peaks and all the shifts agree well with the reported ones from single crystal.[2] Thus, the above tests suggest that the high quality of prepared $Sn_2P_2S_6$ powders, which benefits the structural determination under variable temperatures.

Electric Supplemental Information:

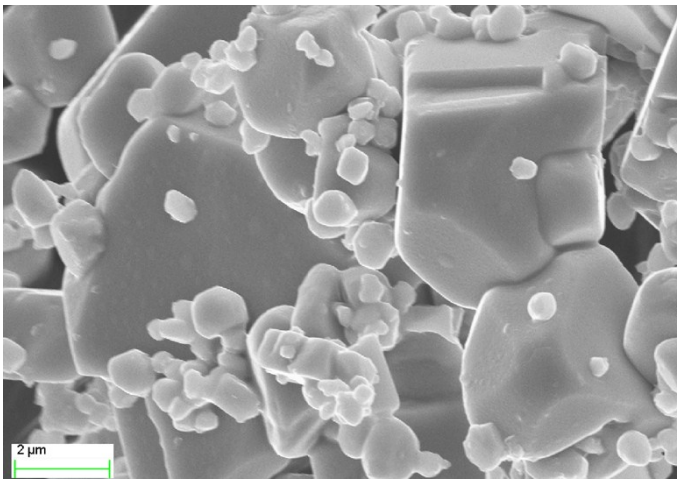

Figure S1. The SEM photo of as-synthesized $Sn_2P_2S_6$ powders.

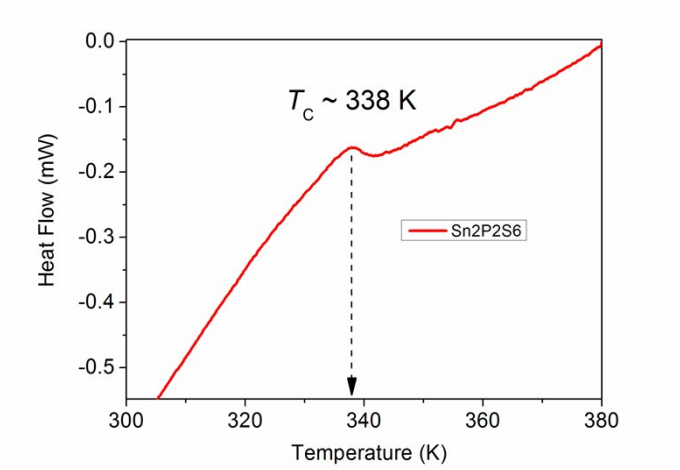

Figure S2. The DSC curve of $Sn_2P_2S_6$ powders between 300 and 380 K.

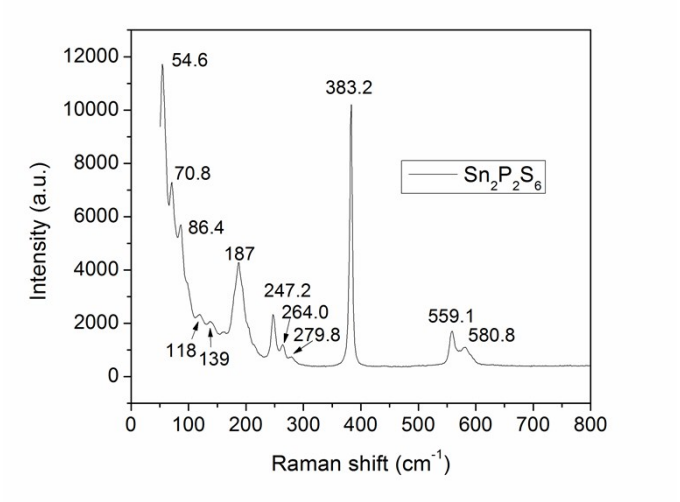

Figure S3. The Raman spectrum of $Sn_2P_2S_6$ powders at room temperature.

Electric Supplemental Information:

3. X-ray diffraction characterizations and Rietveld refinement processing

The X-ray characterizations at non-ambient temperatures were conducted in Anton-Paar TTK 450 chamber, equipped to the Panalytical X'Pert Powder X-ray Diffractometer (Cu Ka, 40 kV and 40 mA). In all measurements, the 2θ step was set to 0.013˚. The measurements were carried out under a vacuum about 0.05 mbar for temperatures below 293 K to avoid freeze and ambient pressure for temperatures from 293 K to 423 K. The heating rate is 10 K/min and all data collections were delayed for 10 min to reach thermal equilibrium. The coppery sample-holder with 0.2 mm depth was used. Patterns of high quality were collected in 2θ range of 13-85 ˚ with 85 minutes per pattern. Total 676 reflections (Ka_2 included) were taken into routine structure refinements using FULLPROF with least squares weighting model. The zero point, background, lattice parameters, atomic positions and isotopic thermal factors were included in the Rietveld refinements. All the refinements were very satisfied with a final R_{wp} below 5 % and χ^2 near 3.0.

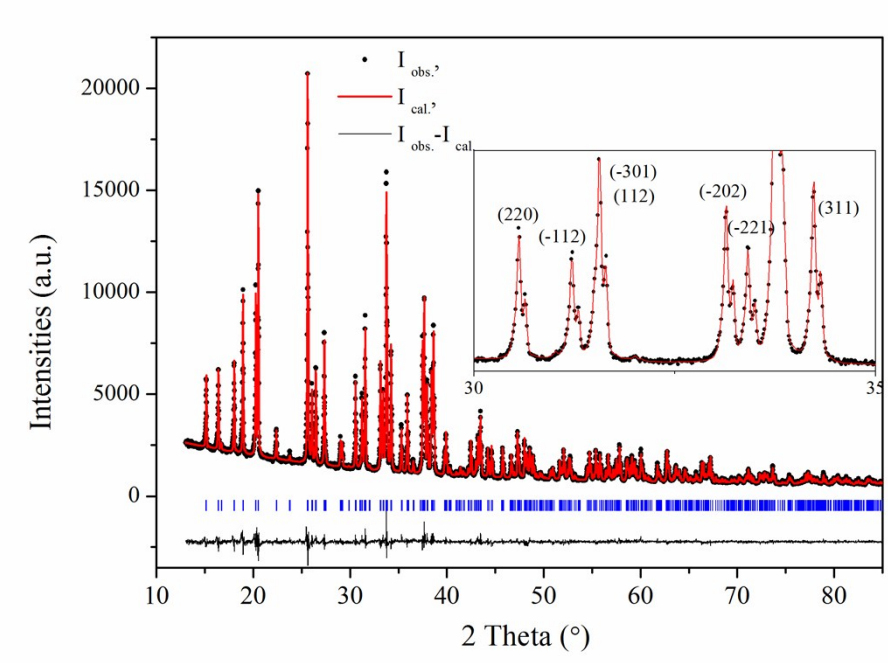

Figure S4. Representative X-ray diffraction pattern of $Sn_2P_2S_6$ powders (293 K). The red line is the calculated result. The inset shows several reflections within 30~ 35°, where the sharp peaks and distinct splits (Ka_1 /Ka_2) suggest high crystallization of as-prepared $Sn_2P_2S_6$ powders.

Electric Supplemental Information:

4. Results of Rietveld refinements

Table S1. Temperature dependent lattice parameters and volume. The goodness factors for the refinements are also listed.

Temp. (K)	Lattice parameters				Volume (Å^3)	Rietveld *R*-factors		
	a (Å)	*b* (Å)	*c* (Å)	*β* (°)		R_p (%)	R_{wp} (%)	χ^2
123	9.38864(7)	7.47524(5)	6.51397(5)	91.0636(3)	457.087(6)	3.49	4.46	3.01
153	9.38746(7)	7.47768(5)	6.51587(5)	91.0742(3)	457.310(6)	3.47	4.43	2.98
183	9.38538(6)	7.47992(5)	6.51753(4)	91.0878(3)	457.460(5)	3.42	4.41	2.95
213	9.38256(6)	7.48190(5)	6.51924(4)	91.1019(3)	457.562(5)	3.39	4.35	2.88
243	9.37869(6)	7.48350(5)	6.52093(4)	91.1178(3)	457.587(5)	3.40	4.45	3.05
273	9.37271(6)	7.48462(5)	6.52261(4)	91.1380(3)	457.478(5)	3.33	4.25	2.77
293	9.36896(6)	7.48411(5)	6.52301(4)	91.1465(3)	457.291(5)	3.30	4.28	2.77
313	9.35919(6)	7.48291(5)	6.52400(4)	91.1740(3)	456.806(5)	3.27	4.24	2.77
333	9.34414(6)	7.47822(5)	6.52439(5)	91.2091(3)	455.807(5)	3.32	4.34	2.87
343	9.33954(7)	7.47600(6)	6.52468(5)	91.2219(3)	455.465(6)	3.59	4.62	2.28
353	9.34193(6)	7.47672(5)	6.52542(5)	91.2222(3)	455.677(6)	3.31	4.29	2.80
373	9.34800(6)	7.47864(5)	6.52722(5)	91.2215(3)	456.216(6)	3.33	4.28	2.80
423	9.36428(7)	7.48366(6)	6.53146(5)	91.2177(3)	457.615(6)	3.24	4.20	2.69

Electric Supplemental Information:

Table S2. The calculated *P*s displacements of Sn(II) cations at variant temperatures. *

Temp. (K)	δ_{Sn1} (Å) (single Sn1-site)		δ_{Sn2} (Å) (single Sn2-site)		Sum δ_{Sn} along *a*-axis	Sum δ_{Sn} along *c*-axis	Total δ_{Sn} of unit cell
	along *a*-axis	along *c*-axis	along *a*-axis	along *c*-axis			
123	0.275(8)	-0.009(9)	0.374(8)	0.157(9)	1.298(8)	0.294(9)	1.331(12)
153	0.273(8)	-0.016(10)	0.372(8)	0.157(9)	1.291(8)	0.281(10)	1.321(13)
183	0.260(8)	-0.016(10)	0.360(8)	0.157(10)	1.240(8)	0.282(10)	1.272(13)
213	0.248(8)	-0.026(10)	0.353(8)	0.157(10)	1.202(8)	0.263(10)	1.231(13)
243	0.233(8)	-0.027(10)	0.339(8)	0.158(10)	1.143(8)	0.262(10)	1.172(13)
273	0.207(9)	-0.044(11)	0.326(9)	0.151(11)	1.067(9)	0.213(11)	1.088(14)
293	0.187(9)	-0.022(12)	0.316(9)	0.178(12)	1.006(9)	0.311(12)	1.053(15)
313	0.155(10)	-0.043(13)	0.297(11)	0.167(14)	0.905(11)	0.247(14)	0.938(18)
333	0.042(13)	-0.066(16)	0.208(14)	0.176(16)	0.500(14)	0.219(16)	0.546(21)

*Calculation methods**:**

Major δ_{Sn1} along the *a*-axis: $\delta_{Sn1}=(x_{Sn1}-\frac{\sum_{i}^{8}x_{S_i}}{8})\times a$; Major δ_{Sn}: Sum δ_{Sn} along *a*-axis

Minor δ_{Sn1} along the *c*-axis: $\delta_{Sn1}=(z_{Sn1}-\frac{\sum_{i}^{8}z_{S_i}}{8})\times c$; Minor δ_{Sn}: Sum δ_{Sn} along *c*-axis

Total δ_{Sn} of unit cell: $\sqrt{(Major\ \delta_{Sn})^2+(Minor\ \delta_{Sn})^2}$

Table S3. Lengths of P-P and P-S bonds under different temperatures. The last three ones are results of paraelectric phase. The (P_2S_6) octahedral seems rather rigid in the ferroelectric phase.

Temp. (K)	P-P (Å)	Maximum P-S (Å)	Minimum P-S (Å)	Average P-S (Å)
123	2.171(7)	2.096(6)	2.002(6)	2.048(6)
153	2.168(7)	2.088(6)	2.010(7)	2.044(7)
183	2.182(7)	2.096(6)	2.002(6)	2.047(6)
213	2.172(7)	2.104(6)	2.009(6)	2.049(6)
243	2.167(8)	2.087(7)	2.012(6)	2.048(6)
273	2.168(8)	2.072(8)	2.018(8)	2.043(8)

Electric Supplemental Information:

293	2.170(9)	2.088(9)	2.018(8)	2.043(8)
313	2.173(11)	2.079(11)	2.003(8)	2.041(10)
333	2.195(13)	2.077(11)	1.980(10)	2.039(11)
353	2.208(2)	2.039(3)	2.021(3)	2.028(3)
373	2.215(2)	2.047(3)	2.015(2)	2.029(3)
423	2.221(2)	2.034(3)	2.021(2)	2.028(3)

Electric Supplemental Information:

5. Comparison of resulted axial CTEs from by dilatometers (literatures) and X-ray diffraction (this work).

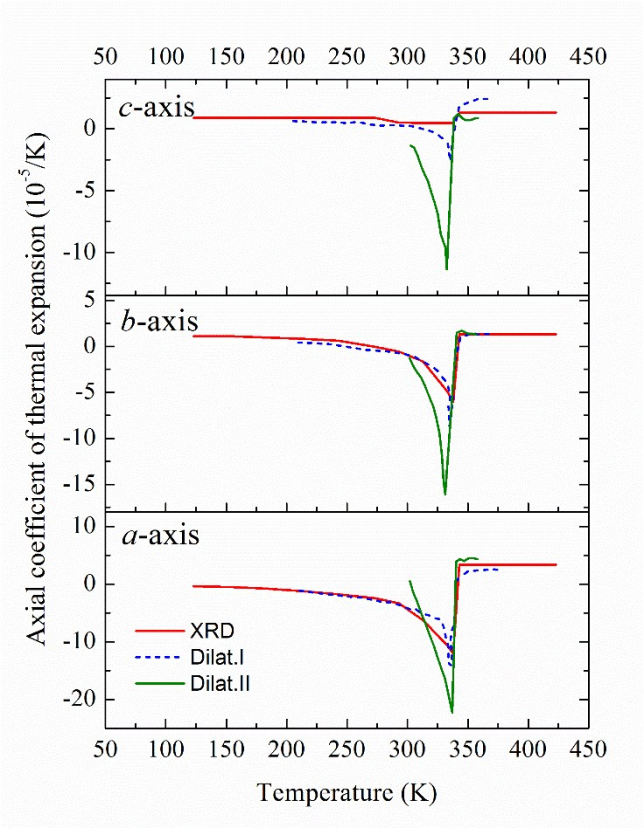

Figure S5. Comparison of axial CTEs obtained by dilatometers (Dilat.) and X-ray powder diffractometer (XRD). The "Dilat. I" is the result reported by Yu. M. Vysochanskii while the "Dilat. II" is the one by A. Say.[3, 4] Note the two results by dilatometers are very different. The "Dilat. I" looks more close to the one by XRD, except the temperature region near the phase transition.

Electric Supplemental Information:

6. First-principle calculations

The First-principle calculations were carried out using projector augmented-wave (PAW) method and Perdew-Burke-Ernzerhof (PBE)-GGA exchange-correlation functional as an implement in VASP.[5, 6, 7] The energy cutoff for the plane-waves is 520 eV and a 7×7×9 *k*-mesh is used.

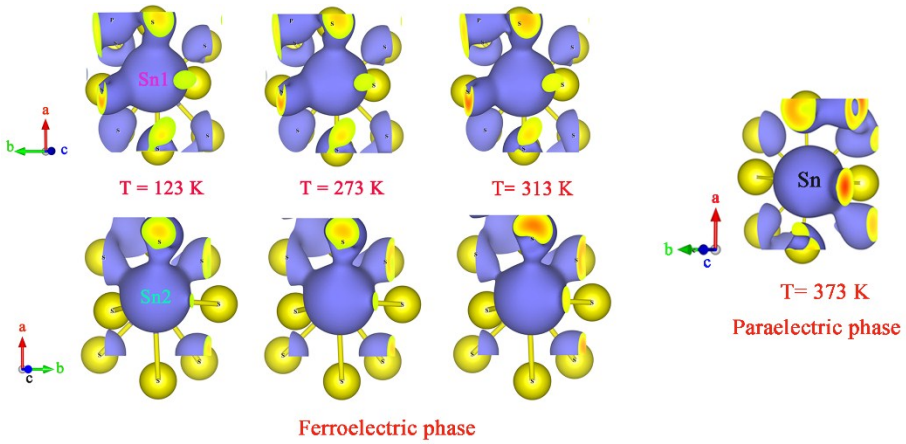

Figure S6. Evolution of the hybridization states in ferroelectric and paraelectric phase, the isosurface is 0.0235 e/Å^3.

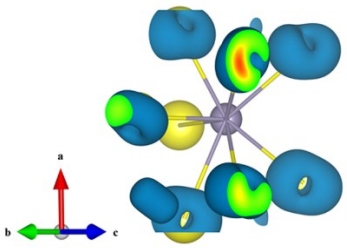

Figure S7. None asymmetrically concentrated electrons around Sn(II) cation could be seen in the paraelectric structure at 373 K, the isosurface is 0.0270 e/Å^3.

Electric Supplemental Information:

Bibliography

1 C. D. Carpentier and R. Nitsche, *Mater Res Bull*, 1974, **9**, 1097–1100.

2 M. B. Smirnov, J. Hlinka and A. V. Solov'ev, *Phys Rev B*, 2000, **6**, 205–212.

3 A. Say, O. Mys, A. Grabar, Y. Vysochanskii and R. Vlokh, *Phase Transit*, 2009, **82**, 531–540.

4 Y. M. Vysochanskii, T. Janssen, R. Currat, R. Folk, J. Banys, J. Grigas and V. Samulionis, *Phase transitions in phosphorous chalcogenide ferroelectrics*, Vilnius University Publishing House, Vilnius, 2008.

5 P. E. Blöchl, *Phys Rev B*, 1994, **50**, 17953.

6 J. P. Perdew, K. Burke and M. Ernzerhof, *Phys Rev Lett*, 1996, **77**, 3865.

7 G. Kresse and J. Furthmuller, *Phys Rev B*, 1996, **54**, 11169.